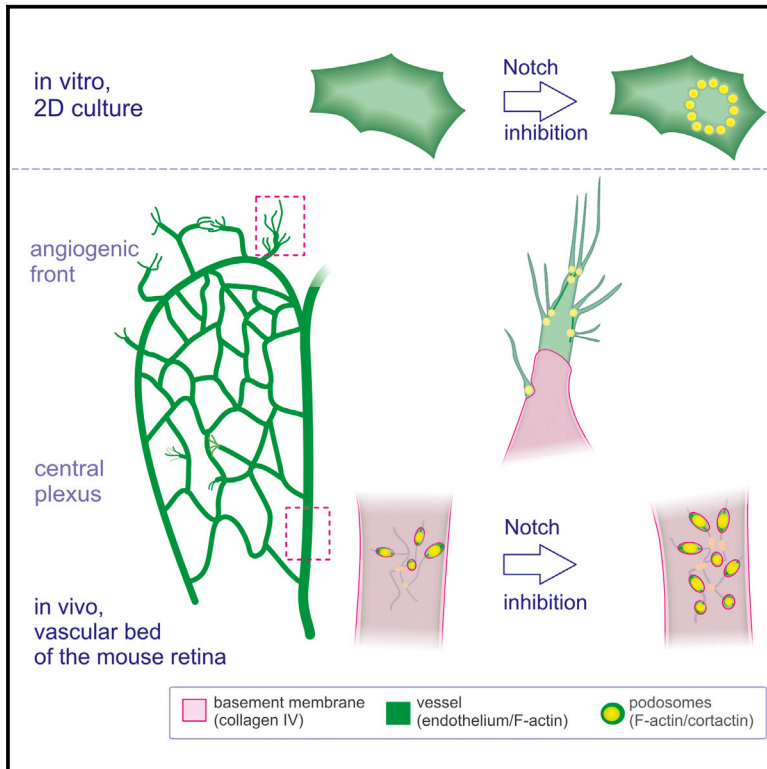# VEGF-A/Notch-Induced Podosomes Proteolyse Basement Membrane Collagen-IV during Retinal Sprouting Angiogenesis

Graphical Abstract

Authors

Pirjo Spuul, Thomas Daubon,
Bettina Pitter, ..., IJsbrand Kramer,
Eloi Montanez, Elisabeth Génot

Correspondence

eloi.montanez@med.uni-muenchen.de
(E.M.),
elisabeth.genot@inserm.fr (E.G.)

In Brief

VEGF-A/Notch signaling orchestrates angiogenic sprouting in a process that requires matrix remodeling by metalloproteases. Spuul et al. now show that, during in vivo angiogenesis, endothelial cells use podosomes to degrade the basement membrane and that Notch signaling restricts endothelial podosome formation in angiogenic vessels.

Highlights

- Endothelial cells form podosomes during developmental physiological angiogenesis

- Podosome formation coincides with loss of collagen-IV vessel coverage

- The VEGF/Notch pathway regulates podosome formation in endothelial cells

- The microenvironment regulates podosome arrangement in angiogenic endothelial cells

VEGF-A/Notch-Induced Podosomes Proteolyse Basement Membrane Collagen-IV during Retinal Sprouting Angiogenesis

Pirjo Spuul,[1,2,4,5] Thomas Daubon,[1,4,6] Bettina Pitter,[3] Florian Alonso,[1,2] Isabelle Fremaux,[1,2] IJsbrand Kramer,[1,2] Eloi Montanez,[3,*] and Elisabeth Génot[1,2,7,*]

[1]Departement Sciences du Vivant et de la Santé, Université de Bordeaux, 146 rue Léo Saignat, 33000 Bordeaux, France
[2]INSERM, U1045, 2 rue Robert Escarpit, 33000 Bordeaux, France
[3]Walter-Brendel Center of Experimental Medicine, Ludwig-Maximilians University, Marchioninistrasse 27, 81377 Munich, Germany
[4]Co-first author
[5]Present address: Department of Gene Technology, Tallinn University of Technology, Akadeemia Road 15, 12618 Tallinn, Estonia
[6]Present address: KG Jebsen Brain Tumour Research Center, University of Bergen, Jonas Lies vei 91, 5009 Bergen, Norway
[7]Lead Contact
*Correspondence: eloi.montanez@med.uni-muenchen.de (E.M.), elisabeth.genot@inserm.fr (E.G.)
 http://dx.doi.org/10.1016/j.celrep.2016.09.016

SUMMARY

During angiogenic sprouting, endothelial tip cells emerge from existing vessels in a process that requires vascular basement membrane degradation. Here, we show that F-actin/cortactin/P-Src-based matrix-degrading microdomains called podosomes contribute to this step. In vitro, VEGF-A/Notch signaling regulates the formation of functional podosomes in endothelial cells. Using a retinal neovascularization model, we demonstrate that tip cells assemble podosomes during physiological angiogenesis in vivo. In the retina, podosomes are also part of an interconnected network that surrounds large microvessels and impinges on the underlying basement membrane. Consistently, collagen-IV is scarce in podosome areas. Moreover, Notch inhibition exacerbates podosome formation and collagen-IV loss. We propose that the localized proteolytic action of podosomes on basement membrane collagen-IV facilitates endothelial cell sprouting and anastomosis within the developing vasculature. The identification of podosomes as key components of the sprouting machinery provides another opportunity to target angiogenesis therapeutically.

INTRODUCTION

Angiogenesis, i.e., the formation of new blood vessels from pre-existing ones, is a vital process during development and tissue regeneration but a major threat in cancer conditions. Blood vessel networks expand in a two-step process that involves sprouting and anastomosis. In the sprouting phase, outgrowing capillaries are guided by specialized endothelial cells (ECs) termed tip cells toward VEGF-A gradients produced by hypoxic

tissues. Tip cells explore their environment by extending dynamic filopodia and migrate in response to VEGF-A signals (De Smet et al., 2009). Concomitantly, neighboring ECs are prevented from doing so and become stalk cells that express relatively lower levels of VEGFR2 than tip cells and proliferate to form the trunk of the neo-vessel. The loops formed by these growing sprouts connect to the rest of the network by anastomosis (Wacker and Gerhardt, 2011).

Tip cells and their interplay with stalk cells have been well described in the developing retinal vasculature of the neonatal mouse. Phenotypically, tip cells are recognizable owing to their polarized nature with prominent filopodia, but they also have a specific molecular signature characterized by the co-expression of the Notch ligand Delta-like ligand-4 (Dll4), the surface adhesion glycoprotein CD34, the axon guidance receptor Unc5B, neuropilin-1, CXCR4, and VEGFR-2 and -3 (del Toro et al., 2010; Strasser et al., 2010). Expression of Dll4 in tip cells suppresses tip-cell fate in neighboring stalk cells via Notch signaling: when Dll4 binds Notch1 on adjacent cells, the cytoplasmic domain of Notch1 is cleaved by γ-secretase and translocates to the nucleus to downregulate VEGFR-2 (Lobov et al., 2007). Consistent with this, tip cells have low levels of Notch signaling activity (Gerhardt et al., 2003; Suchting et al., 2007), and inhibition of Notch signaling stimulates the emergence of tip cells and vascular density (Hellström et al., 2007; Suchting et al., 2007).

By contrast, the events that precede the emergence of the sprout have received little attention. In this first step, the activated ECs must breach the basement membrane (BM) that forms a sleeve around the capillary to escape from the parent vessel. Interestingly, in vitro, VEGF-A induces the formation of matrix degrading organelles, podosome rosettes (rosette-shaped podosome clusters), in human umbilical venous endothelial cells (HUVECs) (Osiak et al., 2005; Wang et al., 2009) and in human microvascular ECs (HMVECs) (Daubon et al., 2016) but not in specific liver sinusoidal ECs (Juin et al., 2013). The latter are derived from hepatic sinusoids that significantly differ from systemic blood vessels as they lack a proper BM
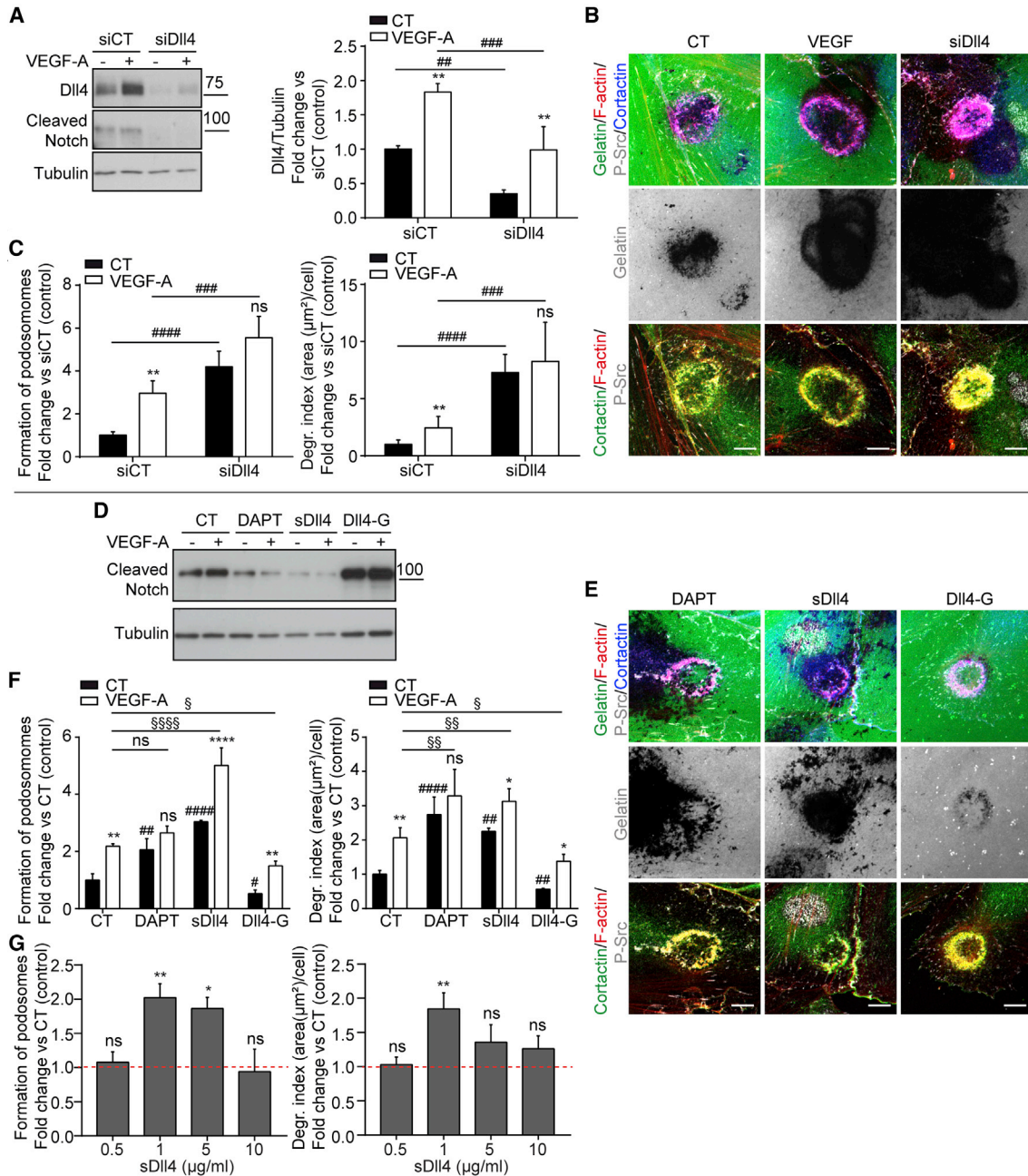
Figure 1. The Notch Pathway Regulates Podosome Formation in HMVECs In Vitro

(A) Reduced expression of Dll4 and cleaved Notch in HMVECs transfected with siDll4. Dll4 expression levels were normalized to tubulin levels (right). One-way ANOVA Bonferroni multiple comparison test was used. Mean ± SD of three independent experiments. ###p < 0. 001, **/##p < 0.01; *compared with the CT in each group.

(B) Representative image of podosome rosettes in untreated, VEGF-A-stimulated or Dll4-depleted cells, triple-stained for F-actin, cortactin, and P-Src and associated Oregon-green-488-conjugated gelatin matrix degradation. Scale bars, 10 μm.

(C) Quantification of podosome formation and matrix degradation in Dll4-silenced cells exposed or not to VEGF-A. One-way ANOVA Bonferroni multiple comparison test was used. n = 3 independent experiments in which 300 cells (for podosome formation) or ten fields (for degradation) were analyzed per experimental point. Data are expressed as fold change compared to siCT, and mean ± SD is shown. ####p < 0.0001, ###p < 0.001, **p < 0.01; *compared with the CT in each group.

(D) Production of cleaved Notch in response to modulation of the Notch pathway.

(E) Representative images of podosome rosettes formed in HMVECs after DAPT or sDll4 addition to the culture medium, or in HMVECs grown on gelatin-containing sDll4 (Dll4-G). Podosomes were visualized as in (B). Scale bars, 10 μm.

(legend continued on next page)

and respond to VEGF-A by dedifferentiation but not angiogenesis (Braet and Wisse, 2002). In vivo, endothelial podosome rosettes regulate vascular branching in tumor angiogenesis (Seano et al., 2014). Podosomes thus appear as likely candidates to act at this stage. However, the relevance of endothelial podosomes in physiological angiogenesis and their integration in the overall process remain unexplored.

So far, most of our knowledge on podosomes comes from studies performed in cells of the myelomonocytic lineage where they are most commonly found. They are described as dynamic cell-matrix contact structures made of a core of F-actin and cortactin surrounded by adhesion molecules and containing matrix-degrading transmembrane MT1-metalloprotease (MT1-MMP) (Linder and Wiesner, 2015). The signaling pathways that involve Src-like kinases and the GTPase Cdc42 converge on the N-WASp-*Arp2/3* axis to promote actin polymerization and subsequent podosome biogenesis (Spuul et al., 2014). In most situations, podosomes arise in groups (Veillat et al., 2015). They constitute the building blocks of clusters organized by a network of actomyosin cables that are also connected to the plasma membrane (Labernadie et al., 2014; van den Dries et al., 2013). In ECs, podosomes are organized in ring-shaped superstructures that are called rosettes (Varon et al., 2006). The observation of collagen-IV (Col-IV)-degrading podosome rosettes in the native endothelium of aortic explants exposed to TGFβ shows that endothelial podosomes subsume specific functions in relation to the BM and supports the physiological relevance of endothelial podosomes in macrovascular cells (Rottiers et al., 2009). We recently showed that microvascular EC podosomes depend on VEGF-A and Col-IV for their induction and function in vitro (Daubon et al., 2016). However, there is as yet no evidence for podosome formation in microvascular ECs undergoing physiological angiogenesis in vivo.

Tip ECs and podosome-forming ECs have been reported independently but share common features. First, Cdc42 controls cytoskeletal rearrangements in both situations since it regulates the formation of the filopodia that characterize tip cells (De Smet et al., 2009; Fantin et al., 2015; Lamalice et al., 2004) and also drives podosome formation (Billottet et al., 2008; Moreau et al., 2006). Second, MT1-MMP is present at the leading edge of invading cells (van Hinsbergh and Koolwijk, 2008; Yana et al., 2007) and is the main proteolytic component of podosomes. In microvascular ECs, VEGF-A regulates endothelial podosome formation whose role in the overall scheme of angiogenesis remains undefined. More particularly, whether podosome induction depends on tip/stack cell specification has not yet been investigated. In a stepwise iterative approach, we explored podosome formation and function in situations that either promoted or forced endothelial specification into tip cells in 2D and 3D organotypic cultures and then in the developing vasculature of the mouse retina. Our results show that VEGF-A/Notch signaling promotes the formation of podosomes in ECs during physiological angiogenesis.

RESULTS

The Notch Pathway Regulates Podosome Formation in Microvascular ECs In Vitro

We used primary HMVECs for these studies as tip cells derive from the specialization of ECs from capillaries. In these cells and in 2D culture conditions, podosomes arise spontaneously in a small fraction (<6%) of the population and are arranged in rosettes at the substrate-attached plasma membrane. When exposed to VEGF-A, the fraction of cells forming podosome rosettes increases up to 15%, and these acquire a higher matrix-degrading potential (Daubon et al., 2016). Interestingly, FGF2, another potent angiogenic inducer, but not hepatocyte growth factor (HGF), also promoted these responses (Figure S1A). Because Notch signaling determines how ECs respond to VEGF-A (Siekmann et al., 2008), we manipulated this pathway to address its role in podosome formation. Silencing the expression of the vascular Notch ligand Dll4 (Hofmann and Luisa Iruela-Arispe, 2007; Shutter et al., 2000) promotes the tip-cell phenotype in a cell-autonomous manner (Sainson et al., 2005). Transfection of HMVECs with small interfering RNA (siRNA) targeting Dll4 effectively reduced Dll4 expression as well as Notch signaling, assessed by the detection of cleaved Notch (Figure 1A). Lowering basal Dll4 levels stimulated podosome rosette formation as detected by F-actin/cortactin/P-Src triple staining (Figures 1B and 1C), and this was associated with increased extracellular matrix (ECM) proteolysis (Figure 1C) as measured in a gelatin degradation assay (Mueller and Chen, 1991). Podosome rosettes induced by Dll4 silencing were found to be similar to those formed in untreated or VEGF-A-stimulated HMVECs (Figure 1B). Thus, inhibition of Notch signals induces cytoskeleton remodeling in ECs. The addition of VEGF-A tended to increase these responses (Figure 1C). To define the direct effect of Notch signaling on podosome formation, the pathway was inhibited by either the pharmacological γ-secretase inhibitor DAPT (N-[N-(3,5-Difluorophenacetyl)-L-alanyl]-S-phenylglycine t-butyl ester) (which blocks Notch cleavage) or by soluble Dll4 (sDll4) (which interrupts Dll4-Notch signaling (Sheldon et al., 2010)). The level of cleaved Notch in response to Notch modulation was verified by western blotting (Figure 1D). DAPT and sDll4 induced similar effects to those produced by Dll4 silencing (Figures 1E and 1F). The podosome response plateaued 1 hr after stimulation, and matrix degradation ensued (Figure S1B). Interestingly, sDll4 was effective in a narrow range with an optimal dose of 1 μg/mL (Figure 1G). Alternatively, the pathway was activated with the Dll4 ligand (immobilized in gelatin to mimic the tethering of the ligand on the cell surface [Caolo et al., 2010]). When seeded on this Dll4-containing

(F) Quantification of podosome formation and matrix degradation in conditions depicted in (E). The statistical analysis was performed as in (C). Data are expressed as fold change compared to CT, and mean ± SD is shown. ****/####/§§§§p < 0.0001, **/##/§§p < 0.01, */#/§p < 0.05; *compared with the CT in each group, #compared with the untreated CT.

(G) Quantification of podosome formation and matrix degradation as a function of sDll4 concentration. The statistical analysis was performed as in (C and F). Data are expressed as fold change compared to CT, and mean ± SD is shown. **p < 0.01, *p < 0.05; *compared with the untreated CT.

See also Figure S1.
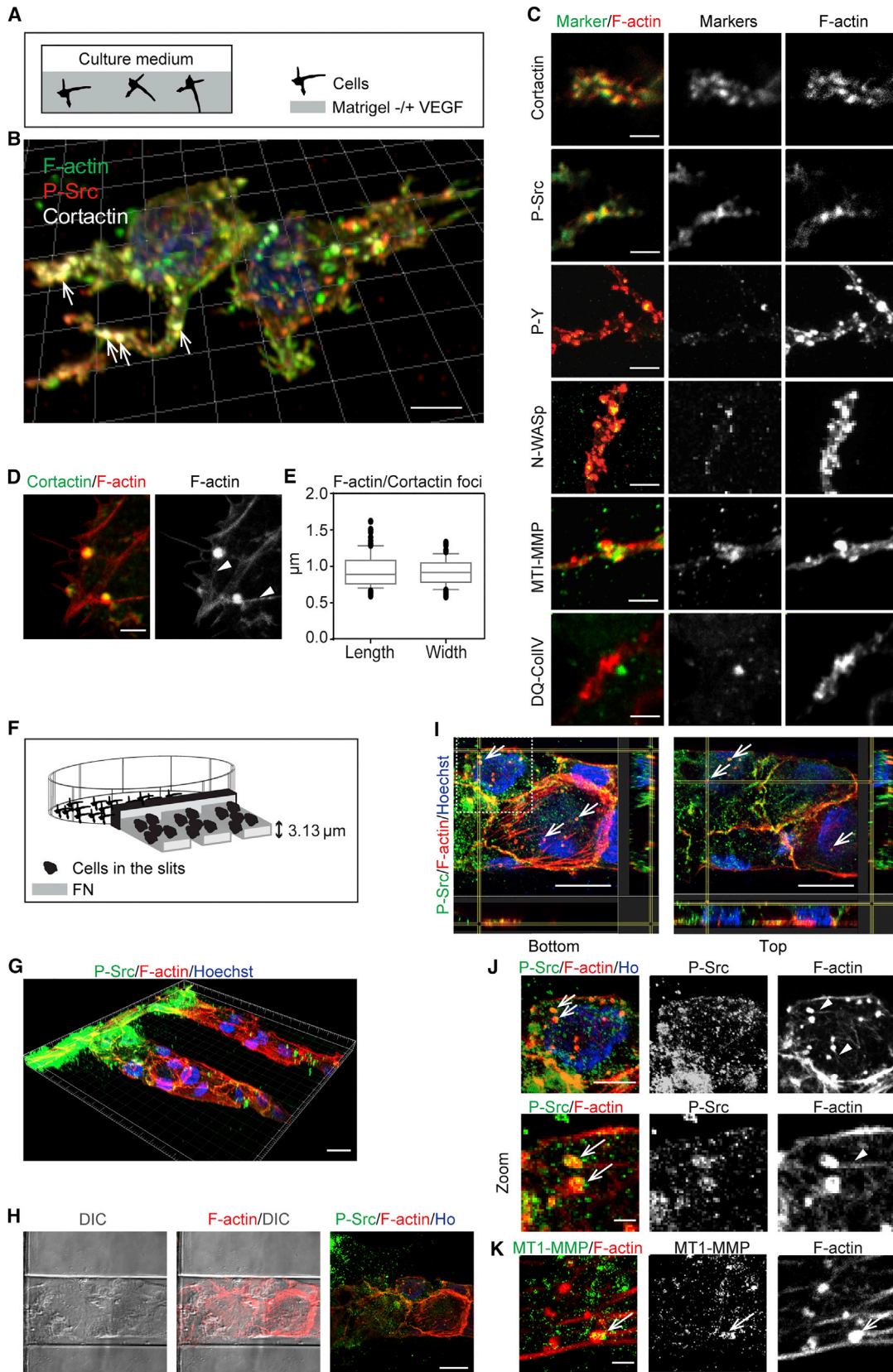
(legend on next page)

matrix, both podosome formation and matrix degradation were reduced in both control and VEGF-A-stimulated HMVECs (Figure 1F). Podosome formation was also reduced when sDll4 was immobilized on plastic surfaces (data not shown). When Notch signaling was inhibited, the amplitude of the VEGF responses increased, approaching but not reaching significance (Figure S1C). To determine how Notch signaling modulation impacted on the matrix degrading function, we examined its effect on cell migration. In contrast to VEGF-A for which the rise in matrix degradation is associated with a stimulation of cell motility that results in more widespread degradation areas (a combination of the higher degradation potential and of the multiplicity of degradation areas associated with the higher motility) (Daubon et al., 2016), the increase in matrix degradation measured for Dll4-depleted cells was associated with a reduced motility. We conclude that the high degradation potential induced by Dll4 depletion produced more focused and deeper degradation areas at podosome sites (Figures S1D–S1F). Altogether, these results show that the Notch pathway regulates podosome formation and function in HMVECs.

Substrate Dimensionality and Spatial Confinement Affect the Architecture and Spatial Arrangement of Podosomes

Having shown the presentation of podosomes in a 2D setup, the next set of experiments addressed podosome formation in a context mimicking the 3D microenvironment that ECs encounter in vivo. We therefore examined podosome architecture and arrangement in HMVECs embedded in Matrigel (a mixture of BM components) containing VEGF-A. In this situation, HMVECs did not show prominent filopodia but formed cellular protrusions (Figures 2A–2C). Triple staining for F-actin/cortactin and P-Src revealed colocalization of the three podosomal markers in globular structures along these cellular extensions. Moreover, MT1-MMP associated with the core structures and other 2D-podosomal proteins were also found in the 3D counterparts. Collagenolytic activity was visualized by the fluorescent staining adjoining the 3D podosomes when (dye-quenched) DQ-Col-IV was included in Matrigel (Figure 2C). The visualization of F-actin cables interconnecting the structures, which requires super-res-

olution imaging (van den Dries et al., 2013), further indicated the identity of podosomes (Figure 2D). Podosomes were about 1 μm in size (Figure 2E).

In tissues, cells have their physical space constrained by neighboring cells and by the ECM. We wondered whether podosomes also formed in HMVECs embedded in tubular structures like they are within patent microvessels, i.e., in non-sprouting contiguous cells behind the angiogenic front. We used microchannels as tubular scaffolds for 3D-confined EC cultures. A microfabricated polydimethylsiloxane (PDMS)-based chip consisting in parallel ∼3-μm-high channels (slits) was coated with fibronectin (FN) (Spuul et al., 2016) an ECM protein required for vascular morphogenesis and matrix deposition (Hielscher et al., 2016; Jiang et al., 1994) (Figure 2F). To highlight the effect of spatial confinement, angiogenic stimulation was reduced by omitting addition of VEGF-A in the medium. Cells were left to migrate on the FN, and, once they had colonized the channels, samples were fixed and imaged. Within the narrow space of the slit, the cells were confluent and formed a pseudo-endothelium (Figure 2G). F-actin/cortactin, F-actin/P-Src, and F-actin/MT1-MMP staining revealed podosomal structures at the basal plasma membrane contacting FN-coated surfaces (Figures 2H–2K). Interestingly, although ECs adhered to the 2D surface of the slit, the podosomes did not form rosettes but appeared as isolated entities interconnected by radiating actin cables.

Thus, VEGF-A induces the formation of endothelial podosomes in a compliant 3D Col-IV/laminin-rich matrix, but their architecture (globular) and arrangement (along cell protrusions) markedly differ from that observed in the 2D setting (rosettes). When HMVECs were aligned in vascular FN-coated 2D tubes, podosomes appeared as interconnected dots at the membrane contacting the underlying matrix. These results show the effects of the ECM microenvironment and geometric confinement on HMVECs on the spatial distribution, architecture, and proteolytic activity of endothelial podosomes.

Tip-Cell-like ECs Display 3D Podosomes

To simulate in vivo sprouting angiogenesis, we set up an assay that mimics the context of tip-cell biogenesis. A Matrigel plug containing VEGF-A was placed in the middle of a culture dish,

---

Figure 2. Substrate Dimensionality Affects the Architecture and Spatial Arrangement of Podosomes

(A) Schematic representation of the setup.

(B) 3D reconstruction from a confocal z stack of a cell embedded in 3D Matrigel, triple-stained for F-actin, cortactin, and P-Src. Scale bar, 5 μm.

(C) Representative images at high magnification of cell protrusions detecting podosomes with their markers together with F-actin. Scale bars, 2 μm.

(D) Interconnecting actin cables between podosomes visualized by STED together with confocal imaging of cortactin. Scale bars, 2 μm.

(E) Quantification of size of F-actin/cortactin foci formed in HMVECs embedded in 3D Matrigel composed of 81 F-actin/cortactin foci from ten cells. Mean ± SD for n = 5 experiments.

(F) Schematic representation of the microfabricated device used to analyze HMVEC cytoskeleton under spatial confinement.

(G) HMVECs when settled into narrow FN-coated slits form a vessel-like endothelium as visualized after triple staining for F-actin, P-Src, and nuclei. Scale bar, 20 μm.

(H) Detail of an individual channel first showing the differential interference contrast (DIC) image, the DIC image merged with the fluorescent F-actin image, and then the triple fluorescent staining (F-actin, red/P-Src, green/ nuclei, blue). Scale bar, 20 μm.

(I) Higher magnification of the section of the pseudo-endothelium shown in (G). Arrows point to podosomes highlighted by F-actin and P-Src staining. Scale bar, 20 μm.

(J) Zoomed image of the boxed region shown in (I) showing podosomes at the contacted FN-coated surface. Arrows point to podosomes highlighted by F-actin and P-Src staining, also shown as single staining. Arrowheads point to F-actin cables interconnecting individual podosomes in the F-actin fluorescence channel image. Scale bar in the upper panel, 10 μm, and in the lower panel, 2 μm.

(K) Representative image illustrating the presence of MT1-MMP at podosomes. Arrow points to the podosome highlighted by F-actin and MT1-MMP staining. Scale bar, 2 μm.
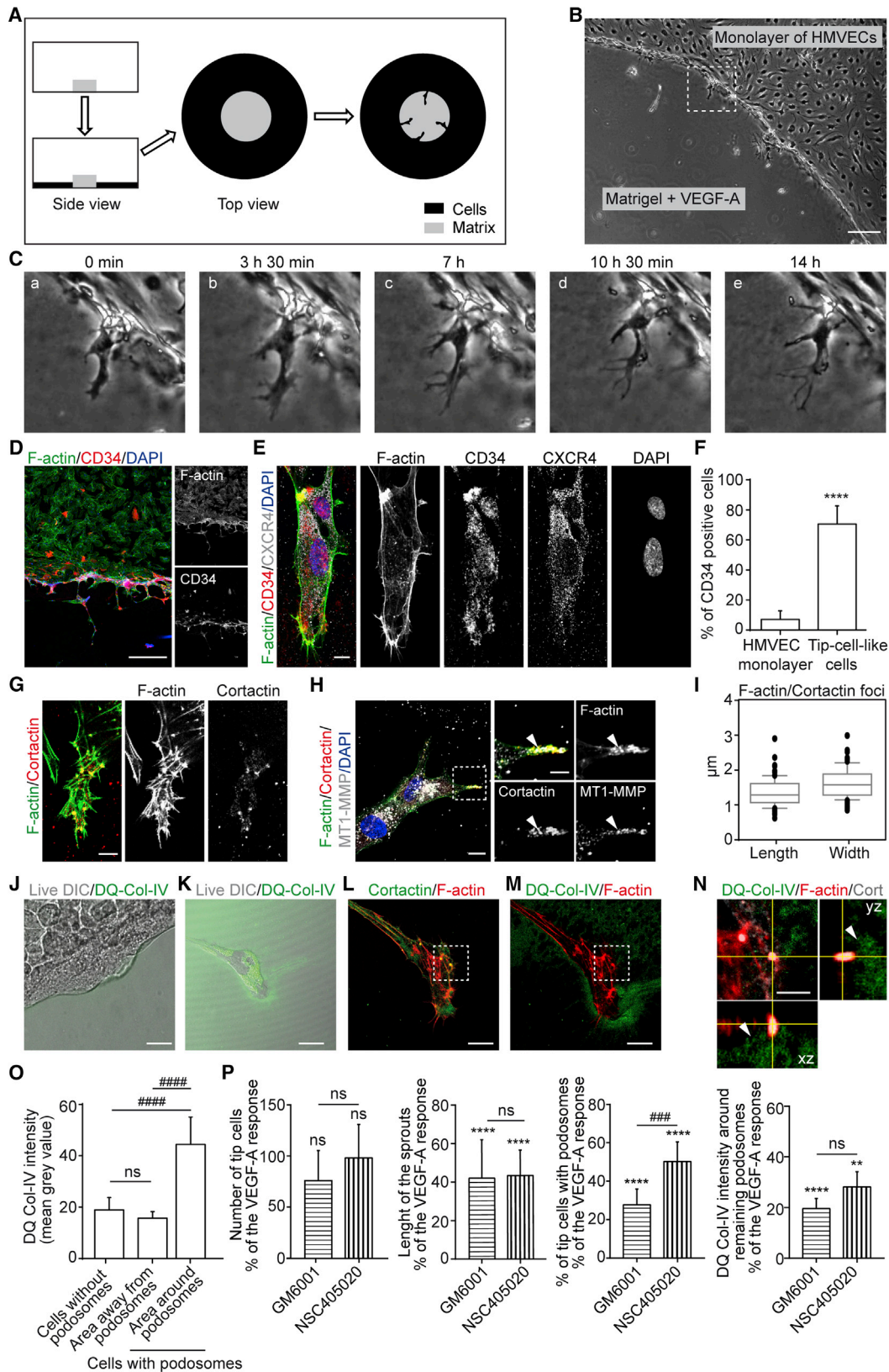
(legend on next page)

and HMVECs were seeded to form a monolayer around it (Figure 3A). At the cell monolayer-Matrigel interface, the ECs were in contact with each other two-dimensionally at their rear and in contact with Matrigel and VEGF-A three-dimensionally at their front (Figure 3B). They were thus confronted by a 3D-barrier that could be penetrated. HMVECs confronted by the 3D-barrier projected filopodia toward the VEGF-A source, invaded the Matrigel (Figure 3C; Movie S1), and expressed the tip-cell markers CD34 and CXCR4 (Figures 3D–3F), suggesting the emergence of tip-cell-like cells. 3D podosomes evidenced by F-actin/cortactin staining were visualized in tip-cell-like ECs (Figure 3G). MT1-MMP staining was strong at podosome areas (Figure 3H). In this setup, the size of the F-actin/cortactin foci (Figure 3I) was comparable to that of 3D podosomes measured in cells embedded in Matrigel (Figure 2E).

We next adapted this assay to assess the collagenolytic activity of 3D podosomes by including DQ-Col-IV in Matrigel. DQ-Col-IV cleavage products were visualized in the pericellular region of cells forming podosomes that were detected after immunofluorescent staining of the same sample (Figures 3J–3N and S2). The DQ-Col-IV fluorescence was higher in the area adjoining podosomes than at distance of them (Figure 3O). These findings suggest that Col-IV was degraded by the proteases exposed by peripheral 3D podosomes in tip-cell-like ECs.

Although MT1-MMP is the main proteolytic component of podosomes, secreted MMPs may also contribute to the observed collagenolytic activity (Linder, 2007). To address this issue, we compared the effect of the general MMP inhibitor GM6001 with that of NSC405020, which presents higher specificity for MT1-MMP (Remacle et al., 2012). In these situations, the outgrowing sprouts led by tip cells were shorter in length, and the number of tip cells with podosomes was reduced, with a more pronounced effect for GM6001 than for NSC405020. The DQ-Col-IV fluorescence associated with the remaining podosomes was markedly reduced in the presence of either inhibitor (Figure 3P). These findings indicate that HMVEC invasion of the Matrigel was mainly dependent on MT1-MMP activity.

To examine the interplay between tip-cell-like cells and podosome-forming cells, we forced the specialization of ECs into tip cells by inhibiting the Notch pathway. For this, we added DAPT together with VEGF-A to Matrigel. Podosomes were found at the periphery of the cell body in cells with filopodia (Figures 4A and 4B). Super-resolution imaging highlighted their interconnection by F-actin bundles (Figure 4C). Podosome distributed with various degree of clustering (Figures 4D and 4E). MT1-MMP staining concentrated in a dot-like pattern in podosome areas with various degrees of overlap with podosomes suggesting the contribution of trafficking vesicles and distinct levels of MT1-MMP enrichment, as described for macrophage podosomes (El Azzouzi et al., 2016; Wiesner et al., 2010). The number of cells with podosomes increased with that of tip cells when Notch was inhibited by DAPT or sDll4 (Figure 4F). Conversely, when tip-cell emergence was prevented by the presentation of exogenous Dll4 immobilized in the Matrigel scaffold (Dll4/Notch

Figure 3. Cells Located at the Monolayer/Matrigel Interface Are Tip-Cell-like Cells
(A) Schematic representation of the setup.
(B) Representative image extracted from Movie S1 showing confluent HMVECs exposed to the Matrigel and VEGF-A gradient in the angiogenesis invasion assay (AIA). Scale bar, 500 μm.
(C) High magnification of representative snapshots extracted from Movie S1, with a zoom on the boxed region shown in (B), taken at 210-min intervals; cells were exposed to Matrigel and VEGF-A at their front project filopodia toward the source, adopting a tip-cell-like phenotype.
(D) The left panel shows a representative immunofluorescent image of cells at the monolayer/Matrigel interface, fixed at day 3 and triple-stained for CD34, F-actin, and nuclei. Individual stainings are shown on the right panels. Scale bar, 500 μm.
(E) A cell protruding in the Matrigel stained for F-actin and CD34/CXCR4 tip-cell markers and individual stainings. Scale bars, 10 μm.
(F) Quantitative analysis of CD34^{+} cell distribution in the monolayer and at tip-cell-like cells. n = 3 independent experiments in which triplicate assays were scored for tip-cell-like cells, and 300 cells were analyzed in the monolayer at the rear per experimental point. Mean ± SD is shown. Student's t test was used. ****p < 0.0001.
(G) A cell protruding in the Matrigel showing F-actin/cortactin foci and individual stainings. Scale bar, 10 μm.
(H) MT1-MMP staining is adjoining the F-actin/cortactin foci in cells protruding the Matrigel. Zoomed area shown in the right panel is indicated with a dashed box. Arrowhead is pointing at the MT1-MMP staining contacting the F-actin/cortactin foci. Note that both intracellular and cell-surface-exposed MT1-MMP are detected. Scale bar, 10 μm, and in the zoomed image, 5 μm.
(I) Size of F-actin/cortactin foci in tip-cell-like cells invading the Matrigel in AIA. 91 F-actin/cortactin foci from 11 cells were analyzed from three independent experiments; mean ± SD.
(J and K) A cell located at the front of the monolayer in the DQ-Col-IV degradation assay. The pericellular Col-IV degradation is visualized in live cells by the fluorescence produced by DQ-Col-IV-FITC cleavage. The micrograph shown in (J) is a merge of the bright-field and DQ-Col-IV fluorescence images, 6 hr after onset and in (K), 3 days later. Scale bar in (J), 20 μm, and in (K), 10 μm.
(L) Confocal projection image of the same sample after fixation and staining for F-actin and cortactin to visualize podosomes.
(M) Correlative image showing the merge of pericellular DQ-Col-IV and F-actin fluorescence images with ongoing pericellular Col-IV degradation around the tip-cell-like cell and the fluorescent degraded matrix at the rear. Scale bars, 10 μm.
(N) Zoom on the boxed region shown in (L and M) showing a merge of pericellular DQ-Col-IV, F-actin and cortactin presented in orthogonal view to visualize the intense DQ-Col-IV signal (arrowhead) in the matrix around podosomes. Scale bar, 5 μm.
(O) DQ-Col-IV fluorescence intensity in the matrix surrounding protruding cells devoid of podosomes and in the matrix surrounding protruding tip-cell-like cells with podosomes (ten cells in each group, n = 3 independent experiments; mean ± SD. One-way ANOVA Bonferroni multiple comparison test was used. ####p < 0.0001. Details of the quantification procedure are shown in Figure S2.
(P) Quantification of vascular sprout parameters in GM6001 or NSC405020 inhibitor-exposed cells. Data are presented as percentage of the VEGF-A response, and mean ± SD is shown. For length measurements, ten sprouts from four independent experiments were analyzed. DQ-Col-IV analysis was performed as specified in (O). One-way ANOVA Bonferroni multiple comparison test was used. ****p < 0.0001, ###p < 0.001, **p < 0.01; *compared with the VEGF-A treated sample.
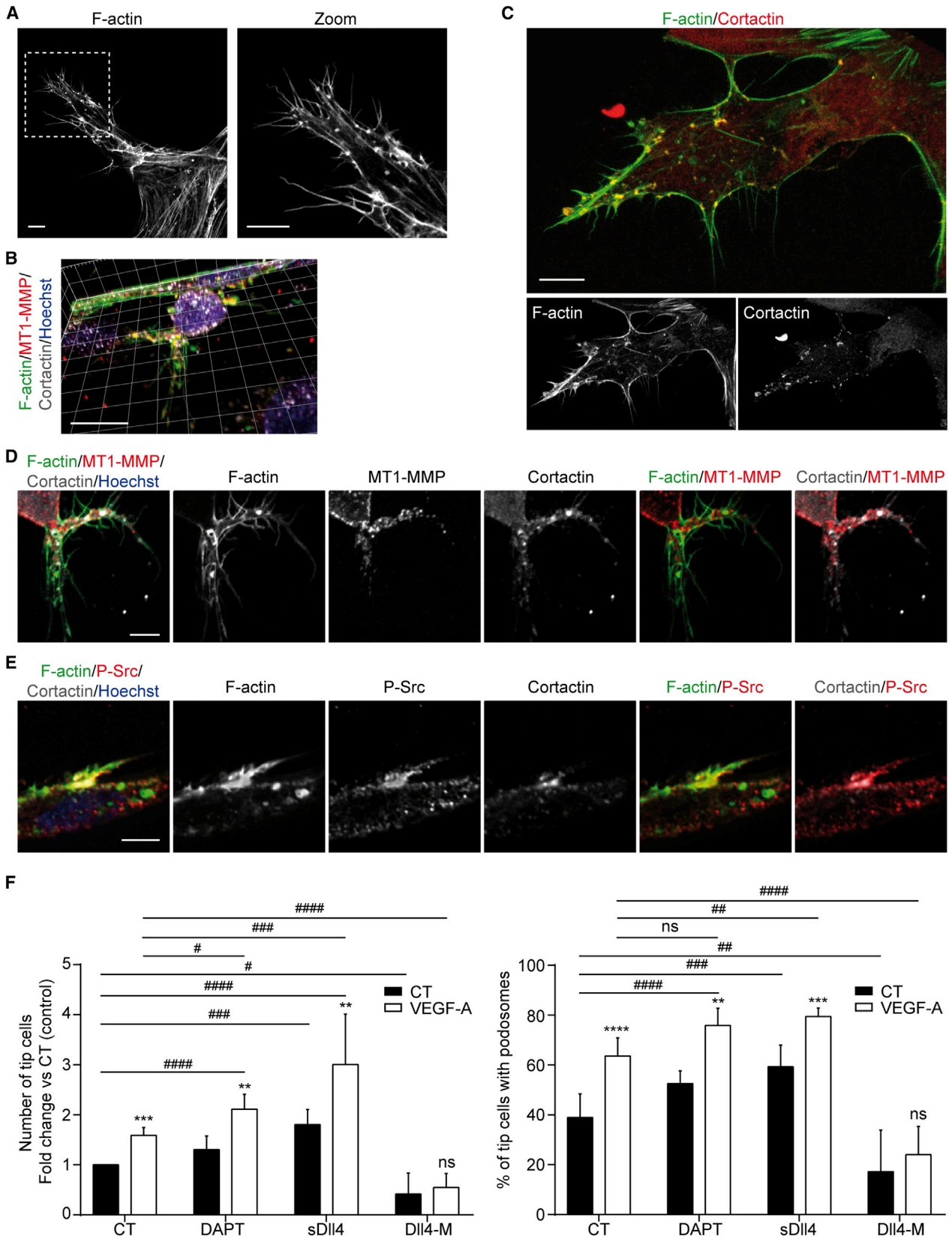
(legend on next page)

signaling was activated), the number of cells with podosomes dropped dramatically (Figure 4F).

Tip Cells Use Podosomes to Degrade the BM Locally during Angiogenesis In Vivo

To address the physiological relevance of our findings, we investigated podosome formation in ECs undergoing sprouting angiogenesis in the mouse postnatal retina. The mouse retinal vasculature develops during the first 3 weeks after birth. In the first week, a primary vascular plexus grows within the ganglion layer of the retina. Guided by a template of FN-expressing astrocytes and following a VEGF-A gradient, this primary plexus expands from the optical stalk toward the periphery of the retina, thereby establishing a 2D vascular plexus. At around postnatal day (P) 8, perpendicular sprouting from the primary plexus leads to the formation of two additional intra-retinal vascular layers in the deeper retina (Potente et al., 2011). We used Lifeact-EGFP-transgenic knockin mice (Riedl et al., 2010) in which the expression of Lifeact-EGFP transgene in the neonatal retina is largely restricted to the endothelium, thereby allowing visualization of the actin cytoskeleton specifically in ECs (Fraccaroli et al., 2012). To study podosome formation, we performed whole-mount immunostaining of P6-Lifeact-EGFP retinas for cortactin, P-Src, Col-IV, and the endothelial marker, isolectin B4 (Figures 5A and S3A). Using confocal microscopy, we observed discrete prominent F-actin/cortactin/P-Src foci at tip cells at the vascular angiogenic front (Figure 5A). The structures distributed at the periphery of the distal tip-cell end or along the cellular protrusions devoid of Col-IV staining were associated with numerous filopodia or formed clusters intermingled with the subcortical actin filaments meshwork (Figures 5A and 5B). Tip cells at the central plexus also displayed F-actin/cortactin/P-Src foci (Figures S3A–S3C). These were arranged in clusters only on rare occasions (Figure S3C), suggesting that this arrangement could be a transient pattern. Remarkably, all foci coincided with gaps in Col-IV staining that were suggestive of proteolytic activity on the ensheathing BM to allow vessel branching (Figures 5A and S3C). The laminin staining was found rather uniform at tip cells (Figures S4A and S4B). In view of these observations, these structures fit the definition of podosomes. The analysis also suggested that tip cells use podosomes to degrade the BM of the neighboring vessel in a process that may favor vessel fusion and anastomosis (Figures 5C and 5D). Most tip cells displayed both podosomes and filopodia (59% of the tip cells contained podosomes (n = 4 retinas)). Together these findings suggest

that tip ECs use podosomes to degrade the BM in the sprouting, branching, and anastomosing steps of angiogenesis in vivo (Figure 5E).

However, we also observed discrete and prominent F-actin/cortactin/P-Src foci in ECs of larger retinal vessels. We focused the analysis on veins for which the analysis appeared more doable as ECs are elongated and spindle shaped in arterioles but larger and polygonal in shape in postcapillary venules. The structures were regularly spaced along the vessel (Figures 6A and S5A) or occasionally arranged in clusters (Figures 6B and S5B). Lack of Col-IV staining in regions of F-actin/cortactin-rich foci was indicative of collagenolytic activity (Figures 6A, 6C, S5A, and S5C) confirming that these structures also corresponded to podosomes (Saltel et al., 2011). Strikingly, F-actin filaments interconnecting podosomes and podosome clusters were highly visible in this setting (Figures 6A and S5A). XZ and XY projections of confocal z stack showed that these F-actin/cortactin foci were associated with the abluminal cell membrane and were penetrating the BM (Figures 6C, 6D, and S5C). Finally, the size of the F-actin/cortactin foci in vivo (Figure S5D) was comparable to that of podosomes measured in the in vitro setups (Figures 2E and 3I). We found that 45% (n = 8 retinas) of the stacks without identifiable tip cells contained podosomes. The distinct arrangement of podosomes in tip cells (Figures 5A–5C) and non-tip cells (Figure 6A) highlights the influence of the microenvironment on the spatial distribution of podosomes in vivo.

At P12, the neovessels cover the entire surface of the retina, and tip cells are no longer detected in the superficial vascular network (Hofmann and Luisa Iruela-Arispe, 2007). To examine whether podosome formation was restricted to the sprouting phase of angiogenesis, we performed immunostaining for cortactin on P9 and P12 Lifeact-EGFP retinas. We observed a gradual reduction in podosome number as angiogenesis in the superficial vascular plexus proceeded to completion (Figure 6F). We found a dramatic reduction in podosome density and the size of the remaining foci was greatly reduced (Figure 6G). These results indicate that podosome formation is associated with active angiogenesis.

The Notch Pathway Regulates Podosome Formation in the Developing Vasculature In Vivo

To study the role of Notch signaling in podosome formation in vivo, Lifeact-EGFP mice were injected subcutaneously with DAPT at P4 and P5, and the retinal vasculature was analyzed

Figure 4. The Notch Pathway Co-regulates Tip-Cell-like Cell and Podosome Formation
(A) Representative image of phalloidin staining in a tip-cell-like EC confronted by the Matrigel plug containing VEGF-A and DAPT. On the right, higher magnification of the boxed region shows filopodia and adjacent F-actin globular structures at the tip. Scale bars, 10 μm.
(B) 3D visualization of maximum projection of entire z stack confocal microscopy images of a tip-cell-like cell located at the Matrigel/monolayer interface (F-actin, cortactin, MT1-MMP). Scale bar, 10 μm.
(C) F-actin/cortactin double staining of a tip-cell-like EC showing podosomes at the cell periphery and interconnecting F-actin cables visualized by STED microscopy. Individual STED (F-actin) and confocal (cortactin) staining are shown below. Scale bar, 10 μm.
(D and E) Various patterns of podosome arrangements in tip-cell-like ECs positive for F-actin, cortactin, MT1-MMP, or P-Src. Note that both intracellular and cell-surface-exposed MT1-MMP are detected. Scale bar, 5 μm.
(F) The number of tip cells with podosomes varies together with the number of tip-cell-like cells when VEGF-A, DAPT or sDll4 was added to the medium, or when Dll4 was immobilized in the Matrigel (Dll4-M). n = 3 independent experiments, mean ± SD. One-way ANOVA Bonferroni multiple comparison test was used. ****/####p < 0.0001, ***/###p < 0.001, **/##p < 0.01, #p < 0.05; *compared to the CT in each group.
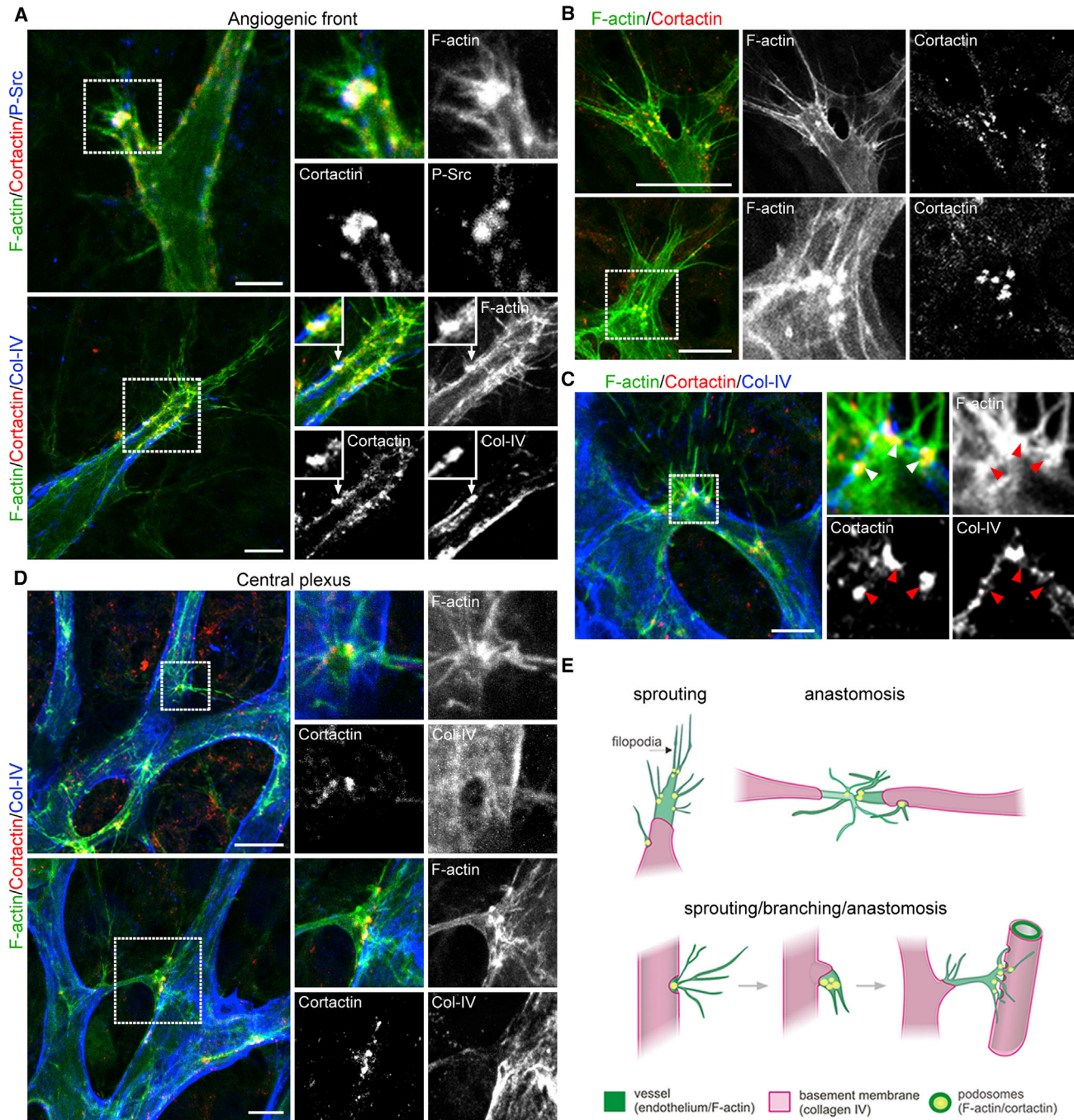
**Figure 5. Tip Cells Use Podosomes to Degrade BM In Vivo**

(A) The vascular front of P6 retina from a Lifeact-EGFP mouse labeled for cortactin and P-Src or for cortactin and Col-IV with zoomed images of the boxed region in the insert. F-actin (Lifeact-EGFP) in ECs appears as bright green. Note that podosomes are visible in a region devoid of Col-IV staining. Scale bars, 10 μm.

(B) High-magnification images of the F-actin/cortactin foci at the tip cells. Scale bar, 10 μm.

(C) Anastomosis of two vessel segments conducted by tip cells. Note the F-actin/cortactin foci at the base of the intermingled filopodia.

(D) P6 Lifeact-EGFP retinas labeled for cortactin and Col-IV, F-actin imaged at the level of the vascular plexus. The boxed regions are shown at higher magnification in the inserts. In the upper panel, note the filopodial extensions emanating from a region with F-actin/cortactin foci (arrow) that is devoid of Col-IV staining. In the lower panel, F-actin/cortactin foci are seen in a protrusion emanating from a tip cell and contacting the neighboring EC. Note the absence of Col-IV staining at the contact zone, matching the F-actin/cortactin foci. Scale bar, 10 μm.

(E) Cartoon depicting podosomes in ECs during vessel sprouting, branching, and anastomosing.

See also Figures S3 and S4.
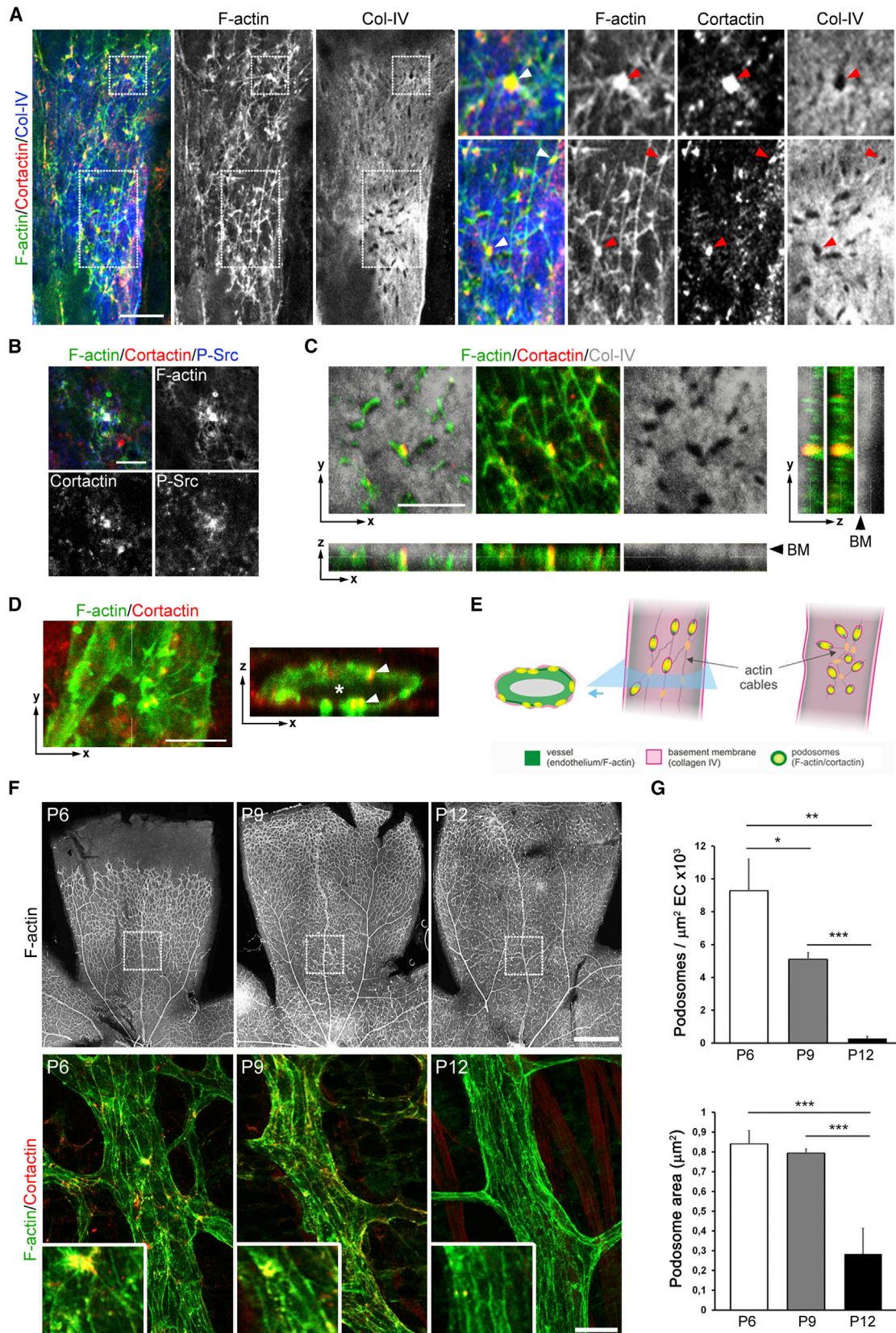
(legend on next page)

at P6. As shown previously (Hellström et al., 2007; Suchting et al., 2007), pharmacological inhibition of the Dll4/Notch pathway leads to increased vascular density as a consequence of increased tip-cell number and EC proliferation (Figures S6A and S6B). Quantitative analysis of podosome formation, normalized to the EC surface to correct for the increased vascular density, was performed in three distinct regions of the retina: in the tip-cell area at the vascular front, in the central plexus region and in larger retinal vessels (Figures 7A–7H). At the vascular front, the treatment enhanced sprouting (Figures 7C and 7F), but, when compared to control retinas, no significant difference in podosome number was found (Figure 7I), consistent with the fact that Notch activity is already low in tip cells. However, at the central plexus and in large vessels, podosome density was significantly increased (Figures 7G–7I). In some areas, podosomes appeared larger than in control retinas, but this may have resulted from the formation of podosome rosettes.

We next evaluated whether the effect of DAPT on podosome number was associated with alterations on Col-IV staining. We focused the analysis on large vessels already ensheathed in a primitive BM to examine the effect of Notch inhibition on podosome activity in ECs. Quantitative analysis of Col-IV staining, normalized to the EC surface to correct for the increased vessel diameter, showed that Col-IV staining was reduced in DAPT versus control retinas (Figures 7J–7L). We therefore concluded that the reduction of Col-IV staining in the distal vasculature coincided with the increased occurrence of podosomes in DAPT-exposed retinal vessels.

DISCUSSION

The characterization of podosomes in microvascular ECs confronted with BM proteins and VEGF-A gradients in 3D situations in vitro enabled us to detect functional 3D interconnected podosomes in tip cells of the developing retinal vasculature. Their formation is controlled by the Notch pathway known to orchestrate cell-fate specification and tissue morphogenesis. Podosomes thus appear as key actors of physiological developmental angiogenesis in vivo.

In HMVEC 2D cultures, we previously characterized two classes of podosomes that are both arranged in rosettes, constitutive and VEGF-A-induced podosomes, which can be discriminated by their increased gelatinolytic capacities (Daubon et al.,

2016). We now show that inhibiting the Notch pathway promotes podosome formation in vitro and in vivo, unraveling a long-sought link between EC specification and actin polymerization. Some indirect evidence already showed that Notch/Delta signaling regulates cytoskeleton-dependent events (D'Souza et al., 2008; Redmond and Ghosh, 2001). In addition, Delta ligands colocalize with actin (Lowell and Watt, 2001). A direct interaction with the actin cytoskeleton is unlikely but Dll4 has PSD-95, Dlg1, ZO1 (PDZ)-binding motifs at its extreme C termini (Pintar et al., 2007), which facilitate interactions with PDZ-containing scaffold proteins (Mizuhara et al., 2005). Future studies on the crosstalk between Notch signaling and RhoGTPases will elucidate how podosome formation is promoted when Dll4 signals are impaired.

We further show that substrate dimensionality and spatial confinement affect podosome arrangement. The development of a 3D angiogenesis assay and the use of a microfabricated device allowed us to bridge the gap between simple monolayer cultures of ECs and the in vivo assay of blood vessel development. In 3D contexts, podosome components cluster at the periphery of ECs, along random cell protrusions to form 3D podosomes resembling those described for macrophages embedded in Col-I gels (Van Goethem et al., 2011). However, during angiogenic sprouting, our in vitro assay showed that 3D podosomes form in the vicinity of filopodia, in polarized protrusions emanating from tip-cell-like ECs contacting BM components and use MT1-MMP as the main metalloprotease to sprout away and invade the matrix. In a microfabricated device in which ECs aligned to form 2D tubes, podosomes formed spontaneously and appeared as interconnected entities at the membrane contacting the underlying matrix. These experimental setups show the spatial arrangement of constitutive and VEGF-A-induced podosomes in ECs exposed to distinct ECM and VEGF-A microenvironments.

We used the characteristic features delineated by the in vitro approaches as a criterion for podosome identification in vivo. The retinal model enabled us to visualize membrane-associated prominent F-actin/cortactin/P-Src foci, i.e., podosomes, in ECs undergoing developmental angiogenesis. At the angiogenic front and vascular plexus, podosomes appeared as globular 3D structures intermingled with microfilamentous actin. We thereby describe single podosomes in the vicinity of filopodia in tip cells, clearly distinct from the podosome rosettes in the

---

Figure 6. ECs in Large Retinal Vessels Contain Podosomes

(A) Vessel of P6 retina from a Lifeact-EGFP mouse labeled for cortactin and Col-IV and F-actin (Lifeact-EGFP). Higher magnification of the boxed areas is shown in the right panel. F-actin/cortactin foci (arrows) appear regularly spaced and interconnected by F-actin cables. Col-IV staining is uniform over the vessel surface but absent in regions corresponding to the F-actin/cortactin foci. Scale bar, 10 μm.

(B) P-Src accumulation at F-actin/cortactin foci of ECs in retinal vessels from Lifeact-EGFP mice. Scale bar, 5 μm.

(C) X-Z and Y-Z projections of a confocal z stack of a region shown in the rectangle box in (A). BM, basement membrane.

(D) X-Z projection of confocal z stacks of retinal vessels from Lifeact-EGFP mice labeled for cortactin. A network of podosomes interconnected by actin cables surround the microvessel. Asterisk highlights the vessel lumen, and arrowheads point to F-actin/cortactin foci. Scale bar, 5 μm.

(E) Cartoon depicting the interconnected network of podosomes surrounding the vessel periphery and the clustering of the podosomes in a rosette-like arrangement.

(F) Lifeact-EGFP retina petals (upper panel) and high-magnification images of large retinal vessels (lower panel) labeled for cortactin at P6, P9, and P12. Scale bars, 400 and 20 μm (lower panel).

(G) Quantitative analysis of relative podosome density and podosome area in large retinal vessels at the indicated locations (boxed region in F). Data are presented as means ± SEM (4 animals per group). One-way ANOVA Bonferroni multiple comparison test was used. $*p < 0.05$, $**p < 0.01$, $***p < 0.001$.

See also Figure S5.
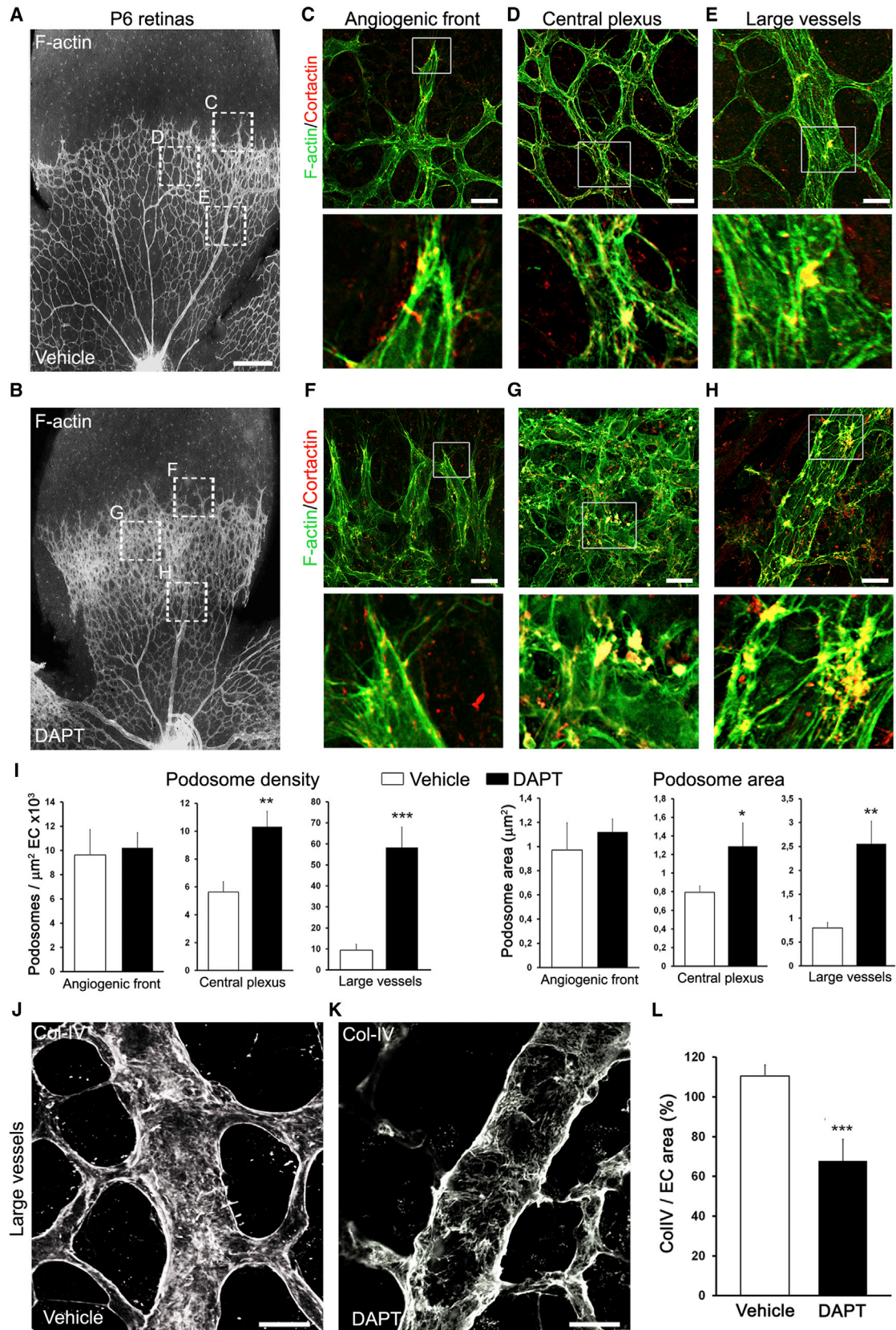
(legend on next page)

distal vasculature reported by Seano et al. (2014). In ECs from large vessels, podosomes appeared as regularly spaced interconnected dots or occasionally appeared in clusters that could be seen as 3D rosette-like arrangements, at the endothelial abluminal plasma membrane. Our in vitro studies using the microfabricated chip that mimics the vessel microenvironment highlight how cell arrangement and geometrical confinement control podosome formation and organization in these regions of presumed low VEGF-A concentrations. Strikingly, in vivo, podosomes were always detected in areas devoid of Col-IV staining, likely reflecting their proteolytic activity. These observations made in distinct ECM and VEGF-A microenvironments support a scenario where the two types of podosomes observed in vitro have their equivalents in distinct regions of the retinal vasculature in vivo. At vessel sprouts, the breakdown of newly synthesized Col-IV at the distal end of tip cells could allow the breakthrough of filopodia and their direct interaction with surrounding FN to enable directional cell migration (Davis and Senger, 2005; Taylor et al., 2015). Indeed, it is known that tip cells are involved in de novo synthesis of BM Col-IV (Bignon et al., 2011) and in its crosslinking by the lysyl oxidase-like protein-2 LOXL2 (del Toro et al., 2010). At contacted BM-ensheathed microvessel sites, local proteolysis of Col-IV could promote direct endothelial cell-cell contacts that allow vessel anastomosis and/or vessel fusion. In these steps, the disruption of the Col-IV bonds loosen the laminin-Col-IV scaffold (Rowe and Weiss, 2008), which subsequently leads to the dissociation of the laminin meshwork (Yurchenco et al., 2004). Our data show significant laminin staining at tip cells supporting the collagenolytic activity of EC podosomes. This scenario would involve adhesive interactions between the tip cells and at the contacted vessel segment and subsequent restoration of Notch signaling upon anastomosis (Estrach et al., 2011; Stenzel et al., 2011). Alternatively, it can also be envisioned that podosome formation is caused by anastomosis. Further experiments are needed to define the role of podosomes during vessel anastomosis.

The role of the interconnected network of podosomes surrounding vessels in ECs of the more distal vasculature remains an open question. At P6, the vasculature of the central retina remodels into an organized structure. The clustering of individual podosomes into rosettes in response to variations in mechanical strains and ECM density in the growing vessel may promote focalized matrix degradation and branching (Edgar et al., 2014). Consistent with this hypothesis, podosome rosettes were seen at vessel branching points where ECs breach the BM in tumoral angiogenesis (Seano et al., 2014). In the neonatal mouse retina, before the primitive 2D vascular plexus reaches the peripheral margin of the retina (around P9), superficial capillaries start sprouting vertically (around P8) to form first the deep and then the intermediate vascular plexus (Hofmann and Luisa Iruela-Arispe, 2007). One intriguing possibility is that the podosome clusters observed in the primary plexus may initiate downward sprouting for invasive progression into the deeper layers of the retina. Regarding the superficial primary plexus at P12, vascular coverage of the retina surface is complete, tip cells have disappeared, and podosomes are no longer detected in this network.

Our observation of podosomes in the retinal vasculature has revealed the existence of a network of actin cables orchestrating podosome arrangement in the native environment. This network likely corresponds to the actin bundles radiating from the actin cores that have been observed in dendritic cells using super-resolution microscopic imaging (van den Dries et al., 2013). Its visualization in the retinal microvasculature without super-resolution imaging reveals its unexpected prominence in situ. The F-actin network that interconnects podosomes thus represents a relevant marker that will facilitate the identification of podosomes in vivo, for instance, in neuronal growth cones, which already share a number of similarities with endothelial tip cells (Santiago-Medina et al., 2015; Tojima et al., 2011).

VEGF-A and Dll4/Notch signaling interact dynamically at the cellular level to control vascular patterning (Jakobsson et al., 2010). How does the Notch/VEGF-A signaling circuit control podosome formation? In tip cells, podosomes were observed to coexist with filopodia and both are known to be regulated by Cdc42. Nonjunctional VE-cadherin, which also triggers Cdc42 stimulation (Kouklis et al., 2003), may provide further activation of the GTPase for the simultaneous occurrence of the two cytoskeletal structures in tip cells. In the remaining vascular network, the pro-angiogenic Notch ligand Jagged-1, which antagonizes Dll4-mediated activation of Notch, is expressed (Benedito et al., 2009; Hofmann and Luisa Iruela-Arispe, 2007), and this pathway may favor podosome formation before these cells become mature stable phalanx cells in which podosomes are no longer formed.

Tip cells are responsible for the formation of new connections. Being equipped with podosomes, the leader tip cell can get rid of the new ECM deposited around the extending sprouts and project filopodia to scan for attractive or repulsive cues and hook on the interstitial matrix. As blood vessels are surrounded by a layer of subendothelial BM, anastomosis also requires local breakdown and/or reorganization of this matrix. In cells of the large vessels, which are still regarded as angiogenic ECs, podosomes may allow some vascular remodeling, while in mature quiescent vessels podosomes are no longer present. Podosome formation should therefore be considered as an integral part of physiological developmental angiogenesis in vivo.

Figure 7. The Inhibition of Notch Signaling Stimulates Podosome Formation and Reduces Col-IV Vessel Coverage in the Developing Vasculature In Vivo
(A and B) A single petal of a P6 retina from vehicle (A) and DAPT (B)-injected Lifeact-EGFP mice. Scale bars, 200 μm. See also Figure S6.
(C–H) High-magnification images from three regions of retinas from vehicle-injected (C–E) and DAPT-injected (F–H); leading front (C and F), central plexus (D and G), and larger vessel (E and H) labeled for cortactin. Scale bars, 20 μm.
(I) Quantification of podosome characteristics in retinal vessels of vehicle and DAPT-injected animals.
(J–L) (J) Col-IV staining of the vessel region shown in (E) (vehicle-injected mice) and (K) Col-IV staining of the vessel region shown in (H) (DAPT-injected animals). (L) Quantification of the Col-IV staining. Scale bar, 20 μm. In (I) and (L), data are presented as means ± SEM (four animals per group). Student's t test was used. *p < 0.05, **p < 0.01, ***p < 0.001 versus vehicle-injected mice.

EXPERIMENTAL PROCEDURES

Mice

Lifeact-EGFP transgenic mice have been previously described (Riedl et al., 2010). Animal procedures were performed in accordance with institutional ethical guidelines. For further details, see Supplemental Experimental Procedures.

Cell Culture and Podosome Assays

HMVECs were cultured in EGM-MV media (Promocell). VEGF-A was used at 25 ng/mL, DAPT at 10 μM, and sDll4 at 1 μg/mL. Podosome formation assays were performed by double staining for F-actin/cortactin or F-actin/P-Src in complete medium. In situ matrix degradation assays were performed as previously described (Varon et al., 2006). For further details, see Supplemental Experimental Procedures.

Microfabricated Devices

Cells were left to migrate in a PDMS-based microfabricated chip containing a series of parallel slits coated with FN for 24 hr. Fixation, staining, and analysis of the cells within the slits were done according to the protocols described previously (Spuul et al., 2016). For further details, see Supplemental Experimental Procedures.

Angiogenesis Invasion Assay and DQ-Col-IV Degradation Assay

In a MatTek dish (MatTek), cells were seeded around a Matrigel plug (containing VEGF-A or VEGF-A + DAPT) to create a BM-like matrix barrier and allowed to invade the plug over a 3-day period at 37°C. To quantitate Col-IV degradation within the plug, DQ-Col-IV was included in and copolymerized with the Matrigel mixture. DQ-Col-IV fluorescence was quantitated at the periphery of cells that had penetrated the Matrigel-DQ-Col-IV mixture at day 3. For further details, see Supplemental Experimental Procedures.

Statistics

Statistical analysis was performed with GraphPad Prism 6 (GraphPad). Significance was determined by using a Student's t test or one-way ANOVA (Bonferroni multiple comparison test between selected pairs), and p values of <0.05 were considered statistically significant.

Additional Procedures

Please refer to the Supplemental Experimental Procedures for details on cell transfection and western bot analysis, whole-mount retina staining, confocal fluorescence imaging, and quantitative analyses.

SUPPLEMENTAL INFORMATION

Supplemental Information includes Supplemental Experimental Procedures, six figures, and one movie and can be found with this article online at http://dx.doi.org/10.1016/j.celrep.2016.09.016.

AUTHOR CONTRIBUTIONS

ACKNOWLEDGMENTS

REFERENCES

Benedito, R., Roca, C., Sörensen, I., Adams, S., Gossler, A., Fruttiger, M., and Adams, R.H. (2009). The notch ligands Dll4 and Jagged1 have opposing effects on angiogenesis. Cell *137*, 1124–1135.

Bignon, M., Pichol-Thievend, C., Hardouin, J., Malbouyres, M., Bréchot, N., Nasciutti, L., Barret, A., Teillon, J., Guillon, E., Etienne, E., et al. (2011). Lysyl oxidase-like protein-2 regulates sprouting angiogenesis and type IV collagen assembly in the endothelial basement membrane. Blood *118*, 3979–3989.

Billottet, C., Rottiers, P., Tatin, F., Varon, C., Reuzeau, E., Maître, J.L., Saltel, F., Moreau, V., and Génot, E. (2008). Regulatory signals for endothelial podosome formation. Eur. J. Cell Biol. *87*, 543–554.

Braet, F., and Wisse, E. (2002). Structural and functional aspects of liver sinusoidal endothelial cell fenestrae: A review. Comp. Hepatol. *1*, 1.

Caolo, V., van den Akker, N.M., Verbruggen, S., Donners, M.M., Swennen, G., Schulten, H., Waltenberger, J., Post, M.J., and Molin, D.G. (2010). Feed-forward signaling by membrane-bound ligand receptor circuit: The case of NOTCH DELTA-like 4 ligand in endothelial cells. J. Biol. Chem. *285*, 40681–40689.

D'Souza, B., Miyamoto, A., and Weinmaster, G. (2008). The many facets of Notch ligands. Oncogene *27*, 5148–5167.

Daubon, T., Spuul, P., Alonso, F., Fremaux, I., and Génot, E. (2016). VEGF-A stimulates podosome-mediated collagen-IV proteolysis in microvascular endothelial cells. J. Cell Sci. *129*, 2586–2598.

Davis, G.E., and Senger, D.R. (2005). Endothelial extracellular matrix: Biosynthesis, remodeling, and functions during vascular morphogenesis and neovessel stabilization. Circ. Res. *97*, 1093–1107.

De Smet, F., Segura, I., De Bock, K., Hohensinner, P.J., and Carmeliet, P. (2009). Mechanisms of vessel branching: Filopodia on endothelial tip cells lead the way. Arterioscler. Thromb. Vasc. Biol. *29*, 639–649.

del Toro, R., Prahst, C., Mathivet, T., Siegfried, G., Kaminker, J.S., Larrivee, B., Breant, C., Duarte, A., Takakura, N., Fukamizu, A., et al. (2010). Identification and functional analysis of endothelial tip cell-enriched genes. Blood *116*, 4025–4033.

Edgar, L.T., Underwood, C.J., Guilkey, J.E., Hoying, J.B., and Weiss, J.A. (2014). Extracellular matrix density regulates the rate of neovessel growth and branching in sprouting angiogenesis. PLoS ONE *9*, e85178.

El Azzouzi, K., Wiesner, C., and Linder, S. (2016). Metalloproteinase MT1-MMP islets act as memory devices for podosome reemergence. J. Cell Biol. *213*, 109–125.

Estrach, S., Cailleteau, L., Franco, C.A., Gerhardt, H., Stefani, C., Lemichez, E., Gagnoux-Palacios, L., Meneguzzi, G., and Mettouchi, A. (2011). Laminin-binding integrins induce Dll4 expression and Notch signaling in endothelial cells. Circ. Res. *109*, 172–182.

Fantin, A., Lampropoulou, A., Gestri, G., Raimondi, C., Senatore, V., Zachary, I., and Ruhrberg, C. (2015). NRP1 regulates CDC42 activation to promote filopodia formation in endothelial tip cells. Cell Rep. *11*, 1577–1590.

Fraccaroli, A., Franco, C.A., Rognoni, E., Neto, F., Rehberg, M., Aszodi, A., Wedlich-Söldner, R., Pohl, U., Gerhardt, H., and Montanez, E. (2012).

Visualization of endothelial actin cytoskeleton in the mouse retina. PLoS ONE 7, e47488.

Gerhardt, H., Golding, M., Fruttiger, M., Ruhrberg, C., Lundkvist, A., Abramsson, A., Jeltsch, M., Mitchell, C., Alitalo, K., Shima, D., and Betsholtz, C. (2003). VEGF guides angiogenic sprouting utilizing endothelial tip cell filopodia. J. Cell Biol. 161, 1163–1177.

Hellström, M., Phng, L.K., Hofmann, J.J., Wallgard, E., Coultas, L., Lindblom, P., Alva, J., Nilsson, A.K., Karlsson, L., Gaiano, N., et al. (2007). Dll4 signalling through Notch1 regulates formation of tip cells during angiogenesis. Nature 445, 776–780.

Hielscher, A., Ellis, K., Qiu, C., Porterfield, J., and Gerecht, S. (2016). Fibronectin deposition participates in extracellular matrix assembly and vascular morphogenesis. PLoS ONE 11, e0147600.

Hofmann, J.J., and Luisa Iruela-Arispe, M. (2007). Notch expression patterns in the retina: An eye on receptor-ligand distribution during angiogenesis. Gene Expr. Patterns 7, 461–470.

Jakobsson, L., Franco, C.A., Bentley, K., Collins, R.T., Ponsioen, B., Aspalter, I.M., Rosewell, I., Busse, M., Thurston, G., Medvinsky, A., et al. (2010). Endothelial cells dynamically compete for the tip cell position during angiogenic sprouting. Nat. Cell Biol. 12, 943–953.

Jiang, B., Liou, G.I., Behzadian, M.A., and Caldwell, R.B. (1994). Astrocytes modulate retinal vasculogenesis: Effects on fibronectin expression. J. Cell Sci. 107, 2499–2508.

Juin, A., Planus, E., Guillemot, F., Horakova, P., Albiges-Rizo, C., Génot, E., Rosenbaum, J., Moreau, V., and Saltel, F. (2013). Extracellular matrix rigidity controls podosome induction in microvascular endothelial cells. Biol. Cell 105, 46–57.

Kouklis, P., Konstantoulaki, M., and Malik, A.B. (2003). VE-cadherin-induced Cdc42 signaling regulates formation of membrane protrusions in endothelial cells. J. Biol. Chem. 278, 16230–16236.

Labernadie, A., Bouissou, A., Delobelle, P., Balor, S., Voituriez, R., Proag, A., Fourquaux, I., Thibault, C., Vieu, C., Poincloux, R., et al. (2014). Protrusion force microscopy reveals oscillatory force generation and mechanosensing activity of human macrophage podosomes. Nat. Commun. 5, 5343.

Lamalice, L., Houle, F., Jourdan, G., and Huot, J. (2004). Phosphorylation of tyrosine 1214 on VEGFR2 is required for VEGF-induced activation of Cdc42 upstream of SAPK2/p38. Oncogene 23, 434–445.

Linder, S. (2007). The matrix corroded: Podosomes and invadopodia in extracellular matrix degradation. Trends Cell Biol. 17, 107–117.

Linder, S., and Wiesner, C. (2015). Tools of the trade: Podosomes as multipurpose organelles of monocytic cells. Cell. Mol. Life Sci. 72, 121–135.

Lobov, I.B., Renard, R.A., Papadopoulos, N., Gale, N.W., Thurston, G., Yancopoulos, G.D., and Wiegand, S.J. (2007). Delta-like ligand 4 (Dll4) is induced by VEGF as a negative regulator of angiogenic sprouting. Proc. Natl. Acad. Sci. USA 104, 3219–3224.

Lowell, S., and Watt, F.M. (2001). Delta regulates keratinocyte spreading and motility independently of differentiation. Mech. Dev. 107, 133–140.

Mizuhara, E., Nakatani, T., Minaki, Y., Sakamoto, Y., Ono, Y., and Takai, Y. (2005). MAGI1 recruits Dll1 to cadherin-based adherens junctions and stabilizes it on the cell surface. J. Biol. Chem. 280, 26499–26507.

Moreau, V., Tatin, F., Varon, C., Anies, G., Savona-Baron, C., and Génot, E. (2006). Cdc42-driven podosome formation in endothelial cells. Eur. J. Cell Biol. 85, 319–325.

Mueller, S.C., and Chen, W.T. (1991). Cellular invasion into matrix beads: Localization of beta 1 integrins and fibronectin to the invadopodia. J. Cell Sci. 99, 213–225.

Osiak, A.E., Zenner, G., and Linder, S. (2005). Subconfluent endothelial cells form podosomes downstream of cytokine and RhoGTPase signaling. Exp. Cell Res. 307, 342–353.

Pintar, A., De Biasio, A., Popovic, M., Ivanova, N., and Pongor, S. (2007). The intracellular region of Notch ligands: Does the tail make the difference? Biol. Direct 2, 19.

Potente, M., Gerhardt, H., and Carmeliet, P. (2011). Basic and therapeutic aspects of angiogenesis. Cell 146, 873–887.

Redmond, L., and Ghosh, A. (2001). The role of Notch and Rho GTPase signaling in the control of dendritic development. Curr. Opin. Neurobiol. 11, 111–117.

Remacle, A.G., Golubkov, V.S., Shiryaev, S.A., Dahl, R., Stebbins, J.L., Chernov, A.V., Cheltsov, A.V., Pellecchia, M., and Strongin, A.Y. (2012). Novel MT1-MMP small-molecule inhibitors based on insights into hemopexin domain function in tumor growth. Cancer Res. 72, 2339–2349.

Riedl, J., Flynn, K.C., Raducanu, A., Gärtner, F., Beck, G., Bösl, M., Bradke, F., Massberg, S., Aszodi, A., Sixt, M., and Wedlich-Söldner, R. (2010). Lifeact mice for studying F-actin dynamics. Nat. Methods 7, 168–169.

Rottiers, P., Saltel, F., Daubon, T., Chaigne-Delalande, B., Tridon, V., Billottet, C., Reuzeau, E., and Génot, E. (2009). TGFbeta-induced endothelial podosomes mediate basement membrane collagen degradation in arterial vessels. J. Cell Sci. 122, 4311–4318.

Rowe, R.G., and Weiss, S.J. (2008). Breaching the basement membrane: Who, when and how? Trends Cell Biol. 18, 560–574.

Sainson, R.C., Aoto, J., Nakatsu, M.N., Holderfield, M., Conn, E., Koller, E., and Hughes, C.C. (2005). Cell-autonomous notch signaling regulates endothelial cell branching and proliferation during vascular tubulogenesis. FASEB J. 19, 1027–1029.

Saltel, F., Daubon, T., Juin, A., Ganuza, I.E., Veillat, V., and Génot, E. (2011). Invadosomes: Intriguing structures with promise. Eur. J. Cell Biol. 90, 100–107.

Santiago-Medina, M., Gregus, K.A., Nichol, R.H., O'Toole, S.M., and Gomez, T.M. (2015). Regulation of ECM degradation and axon guidance by growth cone invadosomes. Development 142, 486–496.

Seano, G., Chiaverina, G., Gagliardi, P.A., di Blasio, L., Puliafito, A., Bouvard, C., Sessa, R., Tarone, G., Sorokin, L., Helley, D., et al. (2014). Endothelial podosome rosettes regulate vascular branching in tumour angiogenesis. Nat. Cell Biol. 16, 931–941, 1–8.

Sheldon, H., Heikamp, E., Turley, H., Dragovic, R., Thomas, P., Oon, C.E., Leek, R., Edelmann, M., Kessler, B., Sainson, R.C., et al. (2010). New mechanism for Notch signaling to endothelium at a distance by Delta-like 4 incorporation into exosomes. Blood 116, 2385–2394.

Shutter, J.R., Scully, S., Fan, W., Richards, W.G., Kitajewski, J., Deblandre, G.A., Kintner, C.R., and Stark, K.L. (2000). Dll4, a novel Notch ligand expressed in arterial endothelium. Genes Dev. 14, 1313–1318.

Siekmann, A.F., Covassin, L., and Lawson, N.D. (2008). Modulation of VEGF signalling output by the Notch pathway. BioEssays 30, 303–313.

Spuul, P., Ciufici, P., Veillat, V., Leclercq, A., Daubon, T., Kramer, I.J., and Génot, E. (2014). Importance of RhoGTPases in formation, characteristics, and functions of invadosomes. Small GTPases 5, e28195.

Spuul, P., Chi, P.Y., Billottet, C., Chou, C.F., and Génot, E. (2016). Microfluidic devices for the study of actin cytoskeleton in constricted environments: Evidence for podosome formation in endothelial cells exposed to a confined slit. Methods 94, 65–74.

Stenzel, D., Franco, C.A., Estrach, S., Mettouchi, A., Sauvaget, D., Rosewell, I., Schertel, A., Armer, H., Domogatskaya, A., Rodin, S., et al. (2011). Endothelial basement membrane limits tip cell formation by inducing Dll4/Notch signalling in vivo. EMBO Rep. 12, 1135–1143.

Strasser, G.A., Kaminker, J.S., and Tessier-Lavigne, M. (2010). Microarray analysis of retinal endothelial tip cells identifies CXCR4 as a mediator of tip cell morphology and branching. Blood 115, 5102–5110.

Suchting, S., Freitas, C., le Noble, F., Benedito, R., Bréant, C., Duarte, A., and Eichmann, A. (2007). The Notch ligand Delta-like 4 negatively regulates endothelial tip cell formation and vessel branching. Proc. Natl. Acad. Sci. USA 104, 3225–3230.

Taylor, L., Arner, K., Engelsberg, K., and Ghosh, F. (2015). Scaffolding the retina: The interstitial extracellular matrix during rat retinal development. Int. J. Dev. Neurosci 42, 46–58.

Tojima, T., Hines, J.H., Henley, J.R., and Kamiguchi, H. (2011). Second messengers and membrane trafficking direct and organize growth cone steering. Nat. Rev. Neurosci. *12*, 191–203.

van den Dries, K., Meddens, M.B., de Keijzer, S., Shekhar, S., Subramaniam, V., Figdor, C.G., and Cambi, A. (2013). Interplay between myosin IIA-mediated contractility and actin network integrity orchestrates podosome composition and oscillations. Nat. Commun. *4*, 1412.

Van Goethem, E., Guiet, R., Balor, S., Charrière, G.M., Poincloux, R., Labrousse, A., Maridonneau-Parini, I., and Le Cabec, V. (2011). Macrophage podosomes go 3D. Eur. J. Cell Biol. *90*, 224–236.

van Hinsbergh, V.W., and Koolwijk, P. (2008). Endothelial sprouting and angiogenesis: Matrix metalloproteinases in the lead. Cardiovasc. Res. *78*, 203–212.

Varon, C., Tatin, F., Moreau, V., Van Obberghen-Schilling, E., Fernandez-Sauze, S., Reuzeau, E., Kramer, I., and Génot, E. (2006). Transforming growth factor beta induces rosettes of podosomes in primary aortic endothelial cells. Mol. Cell. Biol. *26*, 3582–3594.

Veillat, V., Spuul, P., Daubon, T., Egaña, I., Kramer, I., and Génot, E. (2015). Podosomes: Multipurpose organelles? Int. J. Biochem. Cell Biol. *65*, 52–60.

Wacker, A., and Gerhardt, H. (2011). Endothelial development taking shape. Curr. Opin. Cell Biol. *23*, 676–685.

Wang, J., Taba, Y., Pang, J., Yin, G., Yan, C., and Berk, B.C. (2009). GIT1 mediates VEGF-induced podosome formation in endothelial cells: Critical role for PLCgamma. Arterioscler. Thromb. Vasc. Biol. *29*, 202–208.

Wiesner, C., Faix, J., Himmel, M., Bentzien, F., and Linder, S. (2010). KIF5B and KIF3A/KIF3B kinesins drive MT1-MMP surface exposure, CD44 shedding, and extracellular matrix degradation in primary macrophages. Blood *116*, 1559–1569.

Yana, I., Sagara, H., Takaki, S., Takatsu, K., Nakamura, K., Nakao, K., Katsuki, M., Taniguchi, S., Aoki, T., Sato, H., et al. (2007). Crosstalk between neovessels and mural cells directs the site-specific expression of MT1-MMP to endothelial tip cells. J. Cell Sci. *120*, 1607–1614.

Yurchenco, P.D., Amenta, P.S., and Patton, B.L. (2004). Basement membrane assembly, stability and activities observed through a developmental lens. Matrix Biol. *22*, 521–538.